

# Lab on a Chip

Accepted Manuscript



This is an *Accepted Manuscript*, which has been through the Royal Society of Chemistry peer review process and has been accepted for publication.

*Accepted Manuscripts* are published online shortly after acceptance, before technical editing, formatting and proof reading. Using this free service, authors can make their results available to the community, in citable form, before we publish the edited article. We will replace this *Accepted Manuscript* with the edited and formatted *Advance Article* as soon as it is available.

You can find more information about *Accepted Manuscripts* in the [Information for Authors](#).

Please note that technical editing may introduce minor changes to the text and/or graphics, which may alter content. The journal's standard [Terms & Conditions](#) and the [Ethical guidelines](#) still apply. In no event shall the Royal Society of Chemistry be held responsible for any errors or omissions in this *Accepted Manuscript* or any consequences arising from the use of any information it contains.

An optopneumatic piston for microfluidics<sup>†</sup>Juan Rodrigo Vélez-Cordero,<sup>‡a</sup> Misael Giovanni Pérez Zúñiga,<sup>a</sup> and Juan Hernández-Cordero<sup>a</sup>

Received Xth XXXXXXXXXXXX 20XX, Accepted Xth XXXXXXXXXXXX 20XX

First published on the web Xth XXXXXXXXXXXX 200X

DOI: 10.1039/b000000x

We demonstrate an optopneumatic piston based on glass capillaries, a mixture of PDMS-carbon nanopowder, silicone and mineral oil. The fabrication method is based on wire coating techniques and surface tension driven instabilities, and allows for the assembly of several pistons from a single batch production. By coupling the photothermal response of the PDMS-carbon mixture with optical excitation via an optical fiber, we demonstrate that the piston can work either as a valve or as a reciprocal actuator. The death volume of the pistons was between 0.02 and 1.56  $\mu\text{L}$  and the maximum working frequency was around 1Hz. Analysis of the motion during the expansion/contraction of the piston shows that this machine can be described by a phenomenological equation analogous to the Kelvin-Voight model used in viscoelasticity having elastic and viscous components.

## 1 Introduction

We are living an era in which machines are experiencing a reinvention thanks to modern trends in science and technology, such as the human commitment for miniaturization. Although microfluidics and MEMS technologies are developing fields, they have brought several applications and social benefits in the past and promise to expand in areas such as health and digital technology (controlled drug delivery, biosensing, biochemical essays in a chip, cell sorting, cooling systems).<sup>1–5</sup>

Fluid transport and motion at the micro- nanoscale can be generated either passively (minimum or no energy input) or actively<sup>5</sup>. Passive mechanisms offer, in many situations, simple and efficient solutions to transport fluids in microchannels; typical examples are the capillary fluid transport, liquid evaporation or a mixture of both effects<sup>6–8</sup>. Active transport, on the other hand, can be achieved either by moving a boundary or a wall in a reciprocal way, i.e., reciprocal momentum transfer, as done in a pneumatic piston, or by a continuous transfer of momentum<sup>5</sup>. Reciprocal machines are usually complemented with passive valves in order to break the reciprocal motion and generate in conjunction net pumping.

Many different drivers have also been designed in the branch of active transport. Some examples include: human/finger powered pressure driven flows<sup>9,10</sup>, the widely used mechanical pumps such as syringe pumps, and piezoelectric or acoustoelectric high frequency actuators<sup>5</sup>. Flows

can be also generated by active matter such as bacteria carpets<sup>11</sup> or biomolecular motors<sup>12</sup>. Furthermore, optical actuators, either with or without energy conversion, have also proven to be useful as flow drivers<sup>13</sup>.

Most of the flow generators designed during the 90's retain the basic principle of the flexible membrane or diaphragm displacing the fluid back and forth in a cavity. The diaphragm is actuated either by a piezoelectric, electrostatic or electromagnetic device. Similarly, thermal expansion of a gas trapped within a cavity can also be used as an actuation mechanism for the diaphragm (i.e., a thermopneumatic design)<sup>5,14</sup>. An alternative thermopneumatic design was that of Tsai and Lin<sup>15</sup>, based on the reciprocal motion of a bubble expanded and contracted by a heat wave control signal.

The work of Unger *et al.*<sup>16</sup> made an important advance in the design of pneumatic pumps and valves in microfluidics. Using multilayer soft lithography and an external pressure source, they showed that the flow in microchannels can be controlled by pressurizing an adjacent or secondary channel: the obstruction of the primary channel was achieved by deforming a flexible polymer interface between the channels. This pneumatic design has been optimized or automatized since then using flexible interfaces, fluidic diodes<sup>17</sup>, Braille displays<sup>18</sup>, or even the actuation of a simple screw<sup>10</sup>.

Regarding optical actuation, in 2002 Terray *et al.*<sup>19</sup> demonstrated that microvalves and micropumps can be actuated by optical manipulation. Their valves and pumps were made by constructing special arrays of micron sized colloidal beads actuated by a scanning laser. This represented a significant advance towards miniaturization. Since then, several works have shown the capabilities of using optical manipulation in order to move micron sized objects by means of a pump or a valve<sup>13,20–24</sup>. Some of these micromachines work under the prin-

<sup>†</sup> Electronic Supplementary Information (ESI) available. See DOI: 10.1039/b000000x/

<sup>a</sup> Instituto de Investigaciones en Materiales, Universidad Nacional Autónoma de México, Apdo. Postal 70-360, México D.F. 04510, México.

<sup>‡</sup> Present address: Instituto de Física “Manuel Sandoval Vallarta”, Universidad Autónoma de San Luis Potosí, Alvaro Obregón 64, 78000 San Luis Potosí, S.L.P., México; E-mail: jrvelez@ifisica.uaslp.mx

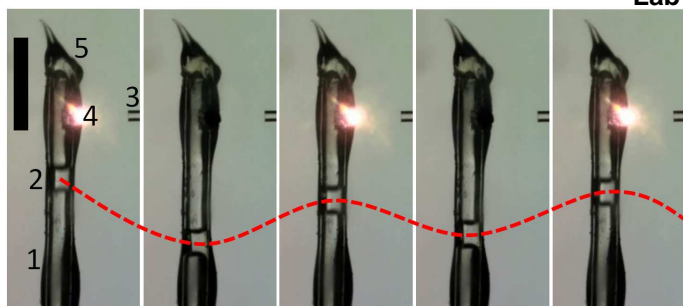


**Fig. 1** Images of the optopneumatic piston showing the position of the droplet when the photoresponsive coating is exposed to periodic light excitation (145.5 mW, 200 mHz). The numbers in the left image denote the parts of the system: 1) glass capillary for piston housing, 2) a mineral oil droplet serves as the “plunger”, 3) optical fiber (125  $\mu\text{m}$ ), 4) photoresponsive coating, 5) silicone seal. The scale bar is 1mm.

ciple of the so-called viscous micropump, which has been described in detail by Day and Stone<sup>25</sup>, and more recently by Matthews and Stokes<sup>26</sup>. In general, optofluidic techniques are very convenient because they combine the best of fluid transport and the best of optics such as fast response times, non-contact actuation, reconfigurability and smooth interfaces<sup>3</sup>.

The optopneumatic piston proposed in this paper works under the same principle as those thermopneumatic actuators having a flexible membrane<sup>27</sup>. We however introduce two important modifications to the basic design, which allows for the reduction of the overall size: 1) heat is generated with a photoresponsive coating while light is guided by an optical fiber; 2) a flexible membrane is replaced by a fluid interface. The resulting driver has intermediate sizes compared to those mentioned so far. As an example, the smallest thermopneumatic driver reported using flexible membranes had an overall volume of 70  $\mu\text{L}$ <sup>5</sup>, and the pump housing of Terray *et al.*<sup>19</sup> was approximately  $1 \times 10^{-6} \mu\text{L}$ . The volume of the optopneumatic pistons reported here range between 0.03 and 1.3  $\mu\text{L}$ . Further advantages of our design include the ease to fabricate the piston using inexpensive materials, easy implementation technologies and mass production possibilities.

## 2 Materials and Methods

### 2.1 Principle of operation and fabrication

The optopneumatic piston works with the principle of isobaric expansion of a gas upon heating. It consist of five components (see figures 1 and 2 for a real image and a schematic representation of the piston): 1) a capillary glass tube that serves as the driver housing, 2) a fluid interface that works as the “plunger”, 3) an optical fiber as the light source, 4) a photore-

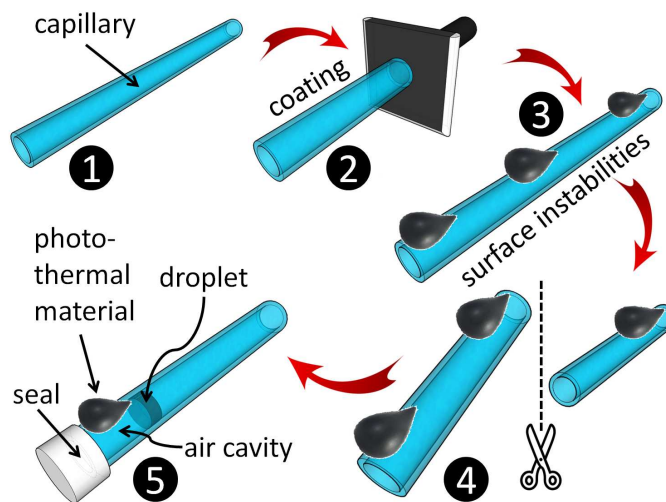


**Fig. 2** Scheme showing the assembling procedure of the optopneumatic piston: a cylindrical glass tube (1) is coated with a photoresponsive composite material (2), the coating layer is left to evolve in a periodic array of individual droplets thanks to surface instability mechanisms (3); when the composite material has solidified, the capillary is cut into several pieces each yielding a different piston (4); finally, each piston is provided with a trapped air cavity using a silicone seal at one end and a fluid interface at the other.

sponsive material that transforms the optical power into thermal energy, and 5) a seal that isolates the gas cavity. Figure 1 shows the displacement of the fluid interface (a mineral oil droplet) when the air in the cavity expands/contracts. Air expansion and heating is achieved by means of the photoresponsive coating layer applied on the outer wall of the capillary. The images in figure 1 show cycles of optical power irradiating the photoresponsive coating. Notice that the reciprocal motion of the droplet is inherent to the driver design, since the confined air contracts to its initial volume  $V_0$  once the optical power is turned off.

Figure 2 shows the methodology followed to assemble the piston. The photoresponsive material is first deposited on the capillaries in a single step by means of a wire coating technique. As reported elsewhere<sup>28,29</sup>, cylindrical shaped tubes such as capillaries can be coated by traversing a reservoir containing a fluid material, usually a polymeric composite, at a certain coating velocity  $U$ . This velocity defines the thickness of the coating,  $h$ , according to the well-known wire coating relation  $h \sim rCa^{2/3}$ , where  $Ca = \eta U / \sigma$  is the capillary number<sup>30</sup>,  $r$  is the external radius of the capillary and  $\eta$ ,  $\sigma$  are the viscosity and surface tension of the coating material, respectively. Therefore, as long as the physical properties of the coating material are known and they remain constant during the coating procedure, the thickness  $h$  of the coating

**Table 1** Characteristics and dimensions of the three pistons designs used in this study. The reported thickness  $h$  correspond to the final measured thickness after the surface instability has grown;  $V_o$  correspond to the death volume or initial air volume trapped in the capillary

| Piston design | Characteristics of the capillaries                                    | Coating velocity $U$ [mm/min] | final thickness $h$ [ $\mu\text{m}$ ] | $V_o$ [ $\mu\text{L}$ ] |
|---------------|---|-------------------------------|---------------------------------------|-------------------------|
| P1            | TrianaTech, wall thickness $65\mu\text{m}$ , $200\mu\text{m}$ I.D.    | 8                             | 95                                    | 0.02                    |
| P2            | TrianaTech, wall thickness $65\mu\text{m}$ , $200\mu\text{m}$ I.D.    | 16                            | 276                                   | 0.04                    |
| P3            | Drummond, wall thickness $135.9\mu\text{m}$ , $629.9\mu\text{m}$ I.D. | 24                            | 266                                   | 1.5                     |

can be predicted and controlled by simply varying the coating velocity  $U$ . It has been shown<sup>29</sup> that this technique can be used for applying coatings on cylindrical geometries from hundreds of nanometers up to millimeters in diameter along several centimeters in the axial direction, thus representing a good alternative in microfabrication techniques.

The coating velocity  $U$  also defines indirectly the characteristic growth time of the Rayleigh-Plateau instability for annular coatings<sup>31</sup> according to the relation  $t^* \sim \eta r^4 / \sigma h^3$ . Such instability constitutes a classical and well studied subject in hydrodynamic stability<sup>32</sup> and relies on a surface energy minimization principle modulated by surface tension. A common example of such instability are the undulations seen in water jets and further breakage into droplets. We deliberately set the velocity  $U$  high enough to yield relatively high values of  $h$  and low values of  $t^*$ . With this settings, we can readily produce, in a single coating step, a periodic array of equally-sized deposits of photoresponsive material along the capillaries (see fig.2 steps 2-3). The distance between the individual deposits along the capillary is automatically scaled by the relation  $\Lambda = 2^{3/2} \pi(r+h)$ , where  $\Lambda$ , in the context of instability theory, corresponds to the wavelength of the most unstable perturbation<sup>31</sup>. This approach was followed to fabricate three pistons with different features (see Table1 for details of the relevant parameters). In the following section, we will show the performance of these pistons as reciprocal actuators.

The photoresponsive material was made by mixing 2.4mg/g of carbon nanopowder ( $< 50\text{nm}$ , Aldrich 633100) in polydimethylsiloxane (PDMS-Sylgard 184, Dow Corning) using a 1:10 ratio of curing agent. Once the coating procedure has finished, the photoresponsive coating is left at room temperature ( $27.5^\circ\text{C}$ ) until the surface instabilities evolve completely (around 10 minutes). Then the coating is heated at  $75^\circ\text{C}$  for 2h until solidification and a glass cutter is used to cut the capillary into several pieces, each having a surface blob of the photoresponsive material (step 4 in fig. 2). Finally, a mineral oil droplet is poured into each piston at a certain distance from one capillary end to be subsequently sealed with silicone (Sista, Dow Corning, general purpose). Two important details regarding this stage of the fabrication procedure are worth mentioning. We used mineral oil as the plunger due to its relatively low contact angle hysteresis with glass

<sup>28</sup>, thereby rendering good slip or low resistance during the expansion/contraction of the trapped air. Note, however, that the real work is carried out by the air cavity and, in general, we can leave aside the plunger and replace it with an interface between the air and a particular fluid intended to be pumped. Secondly, the distance left between the droplet and one of the capillary ends is important and defines the initial volume  $V_o$ . This initial distance  $L_o$  was set arbitrarily and we only took care in matching approximately the value of  $L_o$  with the longitudinal dimension of the coating material given by the surface instability growth. In principle, one can try to solve the variational problem of finding the optimum volume  $V_o$  given certain constrains, such as the energy input or some other fixed spatial dimensions. Yehuda and coworkers<sup>33,34</sup>, for example, computed the maximum work of a piston using the energy conservation equation to derive specific constrains to the variational problem. This however is out the scope of this paper and we only focus on the performance of the pistons.

## 2.2 Power supply and image acquisition

Heating of the photoresponsive material is realized through optical absorption upon irradiating the coating with light from a laser diode ( $\lambda = 975\text{nm}$ ) coupled to an optical fiber (Corning SMF-28e). In contrast with other carbon allotropes, carbon nanopowder is highly available and provides good optical absorption at the wavelength used in our experiments. Notice however that the photoresponsive material could be further optimized upon using other carbon structures with increased absorption such as carbon nanotubes. Similarly, the thickness of the coating layer can be used as another optimization parameter in order to obtain more efficient photothermal responses. Nonetheless, the coatings used in our experiments provided adequate responses to demonstrate photothermal actuation. The optical fiber was placed perpendicular to the capillary wall at a fixed distance of  $500\mu\text{m}$ . The diode controller was connected to a signal generator in order to switch on and off the laser diode at different frequencies  $\omega$ . A digital microscope (DinoLite AD7013MZT) was used for recording videos of the moving plunger, i.e., the mineral oil drop, during the air expansion/contraction. The image resolution was typically  $7\mu\text{m}/\text{pixel}$ , and the velocity measurements or time dependant position of the plunger were evaluated using *ImageJ*.

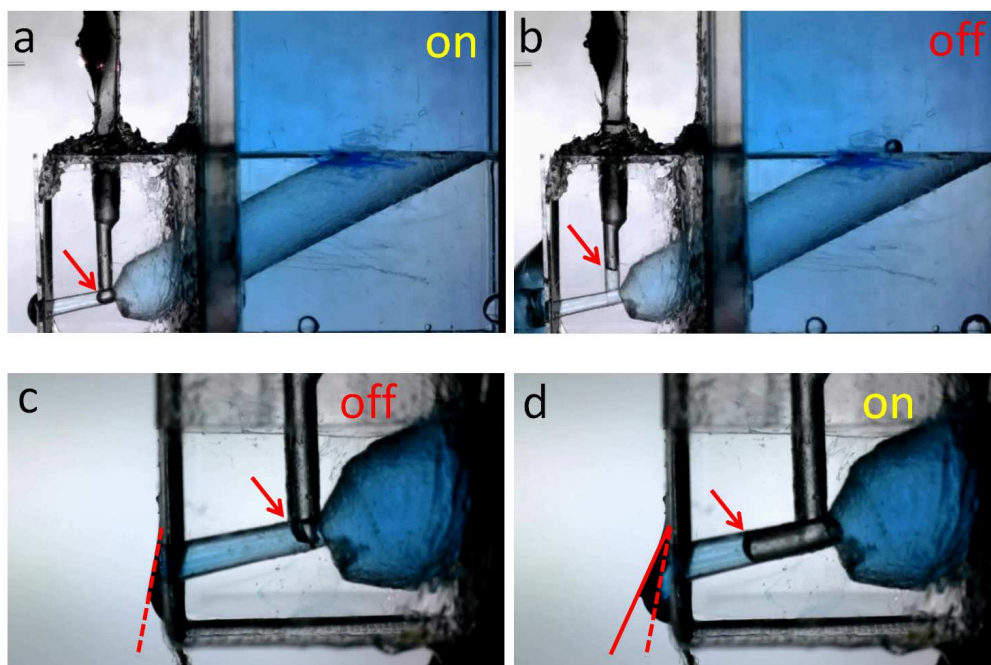


**Fig. 3** The optopneumatic piston working as a valve (a-b) or as a reciprocal actuator (c-d). In the first case, when the gas cavity expands with the heat supplied by the thermoresponsive layer (laser diode on), the air fills an adjacent tube interrupting the flow of the liquid (a); when the laser diode is turned off, the air cavity contracts and the “interfacial gate” is withdrawn from the tube, allowing the fluid to flow. In the second case (c-d), when heat is applied and the air cavity expands, the pushing force is large enough to deflect a PDMS cantilever located outside the tube. These experiments were done with the P3 piston placed vertically in the device. The red arrows denote the position of the moving interface. The optical power used in these experiments was 184.3mW. The colored water is contained in a cuvette having  $1 \times 1\text{cm}^2$  of inner cross sectional area. In the case of the piston working as a valve, the high of the water column was 4cm.

### 3 Results and Discussion

#### 3.1 Operational modes of the optopneumatic piston.

The optopneumatic piston can work either as a valve or as a reciprocal actuator. As shown in Figure 3, the operational mode will depend on the final configuration used when integrating the piston in a microfluidic device. Figures 3a-b show images of the piston working as a valve. In this setup we connected a P3 piston (see Table 1) to a channel connected to a water reservoir (colored with blue stain). When the laser diode is turned on (figure 3a), the air inside the piston expands and fills the adjacent channel at the “T” joint (red arrow). This air expansion works indeed as an “interfacial gate” and as a consequence, the water inside the reservoir is not allowed to flow. When the laser diode is turned off (figure 3b), the air cavity reduces its volume withdrawing the interfacial obstruction inside the channel and allowing the water to flow outside. A video of this case is included in the supplementary material. Figures 3c-d show an example of the piston working as a reciprocal actuator. In this case we attached a cured PDMS membrane outside the channel connecting to the water reservoir. When the laser is turned on (figure 3d), the increase in air volume creates enough thrust to deflect the PDMS membrane; in contrast, when the laser is turned off, the membrane returns to its original position restricting the flow (figure 3c). A video for this case is also included in the supplementary material.

#### 3.2 The optopneumatic piston as an overdamped harmonic oscillator

Figure 4 shows a typical example of the mineral oil droplet displacement as a function of time when the air chamber expands or contracts. The displacement reflects the free expansion of the trapped air when the laser is turned on (heating, square symbols in fig.4) as well as the free contraction when the laser is turned off (cooling, circles in fig.4). In this case, the laser was turned off manually once the maximum droplet displacement was achieved. In all the three different piston designs, and for all the optical powers used in our experiments, the droplet displacement as a function of time,  $L(t)$ , can be modeled as  $L(t) = C_1[1 - e^{-t/C_2}]$  during heating, and as  $L(t) = C_3e^{-t/C_4}$  during cooling. This is interesting because it proves that the micro-piston works, as its macroscopic counterparts, as an overdamped harmonic oscillator, or equivalently, as a Kelvin-Voigt unit with elastic and viscous components, described by the differential equation<sup>35</sup>

$$L + \lambda \frac{\partial L}{\partial t} = C, \quad (1)$$

in which  $\lambda$  is a characteristic relaxation time.

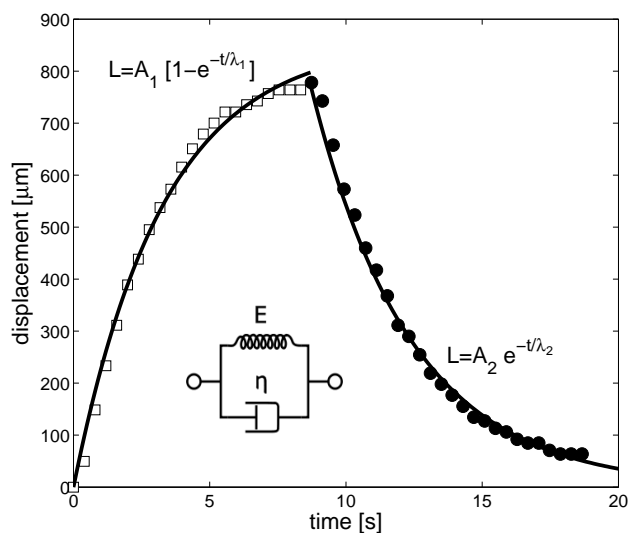


**Fig. 4** Displacement  $L$  of the mineral oil droplet registered in the P1 piston using an optical power of 71.4mW. The symbols denote the heating ( $\square$ ) and cooling ( $\bullet$ ) steps. The droplet displacement during each step can be modeled by the equations shown in the figure, which in turn correspond to solutions of the Kelvin-Voigt unit which has elastic ( $E$ ) and viscous ( $\eta$ ) components (figure included in the plot). Fitting of the curves yielded the following values for this case:  $A_1 = 0.85\text{mm}$ ,  $\lambda_1 = 3.28\text{s}$ ;  $A_2 = 8.3\text{mm}$ ,  $\lambda_2 = 3.66\text{s}$ .

The Kelvin-Voigt model has been used as a simple constitutive model for viscoelastic fluids, and it is formed by connecting in parallel a spring and a dashpot unit (see inset in figure 4). Analysis of the piston motion as a spring-dashpot array, requires us to identify the elastic modulus  $E$  or restitutive force element that imparts memory to the system, and thus returning it to the initial state,  $V_o$ , once the heat source is turned off. Similarly, a relaxation time  $\lambda$  is required to identify the origin of the retardation component that imparts a “viscous” component,  $\eta = \lambda E$ , to the system.

The analogous of the elastic modulus in the piston should be the constant pressure within the channel. Indeed, when the air chamber is heated up, the gas molecules increase their kinetic energy imparting more pressure (molecular collisions) to the walls. Free expansion of the mobile wall, i.e., the droplet, is the system response to keep the initial pressure  $P_o$  constant. The inverse mechanism happens when the system is cooled down: the gas molecules reduce their kinetic energy and the free wall “feels” a vacuum space that equilibrates by reducing the volume. We thus consider that the pressure  $P_o$  represents the constant elastic modulus of the system ( $E = P_o$ ), an approach first posed in the writings of Maxwell.<sup>36</sup>

For the viscous component, fitting of the experimental results yields a relaxation time  $\lambda$  of order  $\mathcal{O}(1)s$ . For comparison, using the air viscosity ( $\eta_{air} \approx 0.02 mPa \cdot s$ ) and a pressure  $P_o \approx 1 \times 10^5 Pa$  yields a relaxation time  $\lambda$  of  $2 \times 10^{-10} s$ . Clearly, the viscous component of the system does not correspond to that of air. Van de Pol *et al.*<sup>14</sup> have mentioned that the motion of optopneumatic devices are governed by a thermal relaxation time. Let us follow a simple argumentation using the energy conservation equation in order to elucidate the origin of this thermal relaxation. The energy conservation equation of the system can be written as<sup>34</sup>

$$\dot{U}(t) = \dot{Q}(t) - \dot{W}(t) - K[T(t) - T_{ex}], \quad (2)$$

where  $\dot{U}(t)$  is the rate of change of the internal energy of the piston,  $\dot{Q}(t)$  is the rate of heat applied to the system,  $\dot{W}(t)$  is the instantaneous rate of work done by the piston, and the term  $K[T(t) - T_{ex}]$  dictates the energy exchange rate between the piston and the environment having an external temperature  $T_{ex}$ ;  $T(t)$  is the instantaneous temperature of the piston and  $K$  is an overall heat transfer rate (in units of Watts per Kelvin). Using  $\dot{W}(t) = P_o \dot{V}$  and the equations of state of an ideal gas,  $\mathcal{U} = nC_v T$ ,  $T = PV/nR$ , eq.2 can be written as:

$$\dot{V}(t) + \frac{K}{n[C_v + R]}V(t) = \frac{R}{P_o[C_v + R]}[\dot{Q}(t) + KT_{ex}]. \quad (3)$$

Solving for the volume  $V(t)$  we get:

$$V(t) = e^{-\frac{K}{n[C_v + R]}t} \frac{R}{P_o[C_v + R]} \int_0^t e^{\frac{K}{n[C_v + R]}t} [\dot{Q}(t) + KT_{ex}] dt + C e^{-\frac{K}{n[C_v + R]}t}. \quad (4)$$

Inspection of eq.4 shows that even for the cases when the function  $\dot{Q}(t)$  acquires an instantaneous form, such as the delta function,  $V(t)$  is still a continuous function of time thanks to the energy exchange with the environment defined by the heat transfer parameter  $K$ . It is therefore this energy exchange that constitutes the analogous of the retardation element or dashpot in the piston and hence participates in defining the thermal relaxation time through the term  $n[C_v + R]/K$  (note that if the piston is thermal isolated,  $K = 0$  and the relaxation time is infinite).

Having identified the spring and the dashpot components of the piston with the air pressure  $P_o$  and the corresponding thermal relaxation time  $\lambda$ , the proposed phenomenological model can be written as:

$$L + \lambda \frac{\partial L}{\partial t} = \frac{q}{P_o}, \quad (5)$$

where  $q$  is the applied heat per unit area. The advantage of using this simple expression, albeit of knowing the values of  $\lambda$  and  $q$ , is that the behavior of the piston can be predicted for several forms of the applied heat  $q$ . For instance, suppose that  $q(t)$  takes the form of a positive sinusoidal function starting from zero, i.e.  $q(t) = q_o(1 - \cos \omega t) = q_o - q_o \mathcal{R}e\{e^{i\omega t}\}$ , where we have used complex notation and where  $\omega$  is the frequency of the heat excitation. Taking a reference value of  $q(t)$  in the form

$$q_{ref}(t) = q(t) - q_o = -q_o \cos \omega t = -q_o \mathcal{R}e\{e^{i\omega t}\}, \quad (6)$$

and proposing a solution for the reference displacement in the form  $L_{ref}(t) = \mathcal{R}e\{\tilde{L}_{ref} e^{i\omega t}\}$ , we obtain after substitution in eq.5:

$$\tilde{L}_{ref} = -\frac{q_o(1 - i\omega\lambda)}{P_o(1 + \omega^2\lambda^2)}. \quad (7)$$

The solution for  $L_{ref}(t)$  can thus be written as:

$$L_{ref} = -\frac{q_o|r|}{P_o(1 + \omega^2\lambda^2)} \cos(\omega t + \varphi), \quad (8)$$

where the modulus and the argument are  $|r| = \sqrt{1 + \omega^2\lambda^2}$  and  $\varphi = \tan^{-1}(\lambda\omega)$ , respectively. The piston will behave therefore similar to other systems, such as electrical or hydraulic circuits, that have an inherent characteristic response time and are excited by a sinusoidal wave input: for low frequency values  $\omega$ ,  $\varphi \approx 0$  and  $L_{ref}(t)$  will be in phase with the excitation wave  $q_{ref}(t)$ . However, for high values of  $\omega$ ,  $\varphi \approx \pi/2$  and  $L_{ref}(t)$  will be out of phase and in opposite direction with respect to  $q_{ref}(t)$ .

### 3.3 Interplay between piston size and response time

Figures 5a and b show the maximum displacements and velocities  $v_{max}$  of the droplet, respectively, as a function of the opti-

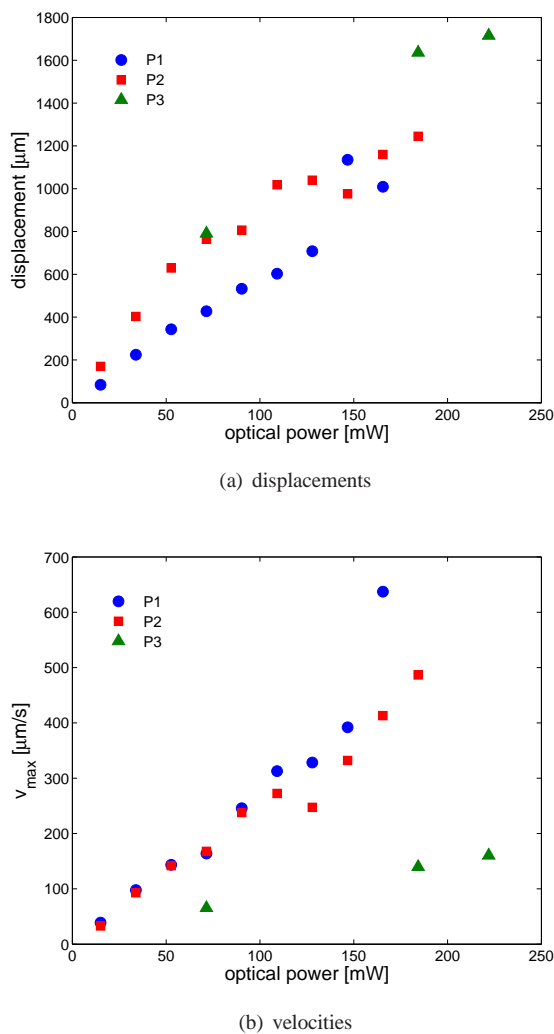


**Fig. 5** Maximum displacements and velocities of the oil droplet as a function of the optical power measured in the three piston designs (see Table 1).

cal power (without wave modulation) for the three piston designs described in Table 1. Figure 5a shows that the maximum displacements increase with the value  $V_o$  of the pistons. This is an expected behavior as long as the heat source is enough to increase the temperature of this initial air volume (recall that the amount of photoresponsive material deposited on the capillaries scales automatically with the capillary size thanks to the coating technique). In contrast, Figure 5b shows a different trend since the maximum velocities correspond to the smaller piston. A smaller thickness of the capillary wall together with a reduction of the photoresponsive layer thickness imply a faster transmission (conduction) of the heat towards the air cavity. Hence, it seems that in terms of the speed or response times, miniaturization in general improves the performance of these kind of devices, as mentioned by Terray *et al.*<sup>19</sup>.

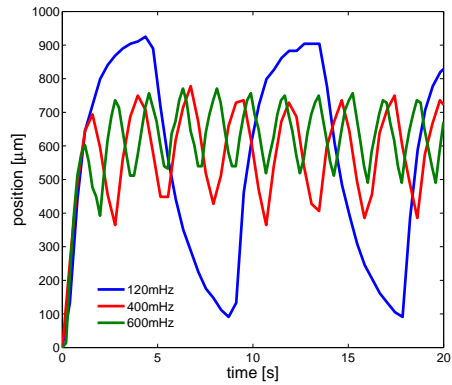
Let us define the efficiency of the optopneumatic piston as:

$$Eff = \frac{P_o v_{\text{max}} \mathcal{A}}{\mathcal{P}} \quad (9)$$

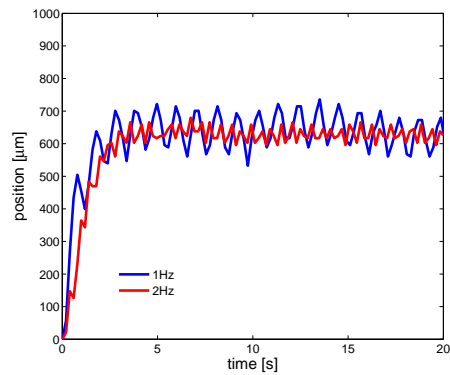
where  $\mathcal{A}$  is the cross sectional area of the capillaries,  $\mathcal{P}$  is the optical power and  $P_o$  can be calculated using the ideal gas formula  $P_o = \rho R T_o / PM$ ,  $\rho$  being the density of air ( $\sim 1174 \text{ g/m}^3$ ),  $T_o$  the initial temperature (300.65 K) and  $PM$  the molecular weight of air (28.97 g/mol). The maximum efficiency found in our experiments, which correspond to that obtained for the P1 piston, is in the order of  $1 \times 10^{-3}\%$ . For comparison, the highest efficiencies reported for other thermopneumatic actuators<sup>5</sup>, already coupled to passive valves, is around  $4 \times 10^{-5}\%$ . Although the efficiency is clearly improved in the present device, coupling of the piston with passive valves is still required to fully compare its performance with previous reports. Note that the value of the efficiency can be also estimated upon fitting the experimental values to the solution of eq. 5, i.e.  $L = q_o / P_o [1 - e^{-t/\lambda}]$ . Once the value of the effective heat,  $Q_o$ , is known, which is equal to  $q_o$  times an area for heat transfer, one can compare this value to the total energy applied to the system, which is equal to the optical power  $\mathcal{P}$  multiplied by the time the laser diode was kept on. Using this calculation the approximated value of the efficiency was found to be around  $1 \times 10^{-2}\%$ . The obtained efficiency falls within typical values of those obtained in systems performing energy conversion for heat production. Nonetheless, this may be improved upon optimizing the response of the coating and/or the light delivery arrangement.

### 3.4 Performance of the optopneumatic piston at different excitation frequencies $\omega$

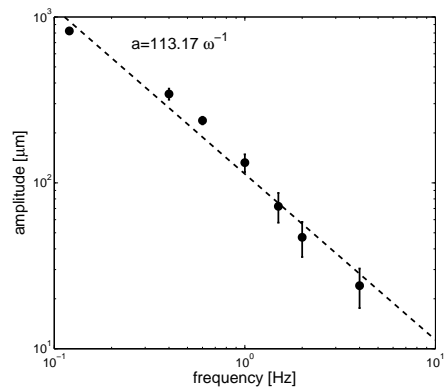
Figure 6 shows the droplet displacement in the piston P1 (the one that yielded the largest droplet velocities), at different excitation frequencies  $\omega$ . The excitation signal is obtained upon



(a) 120, 400 and 600 mHz



(b) 1 and 2 Hz



(c) amplitude vs frequency

**Fig. 6** Displacement of the oil droplet as a function of time for the P1 piston at different excitation frequencies  $\omega$ . Figure (c) shows the amplitude of the drop displacement as a function of the frequency, the curve is fitted by the relation  $a = 113.17\omega^{-1}$ . The optical power in all cases was 154.5mW.

modulating the laser diode coupled to the optical fiber using an external control signal. The supplementary information includes a video showing the piston performance at different frequencies spanning 120mHz to 4Hz. Figures 6a and b show the oscillatory displacement of the droplet and the corresponding reduction of the displacement amplitude,  $a$ , as the frequency increases. Figure 6c shows that the amplitude of the oscillations is proportional to the inverse of the frequency, i.e.,  $a \sim \omega^{-1}$ .

This indicates that the piston indeed works according to the rules dictated by the viscoelastic model, eq.5. We showed that the solution of this equation for periodic excitations, eq.8, predicts responses in phase or out of phase with respect to the excitation wave depending on the values of  $\omega\lambda$ . Besides this time dependence of the displacement, eq.8 further predicts a displacement reduction (i.e., a decrease in amplitude) due to the factor  $(1 + \omega^2\lambda^2)^{-1/2}$ , which for  $\omega\lambda > 1$ , yields the observed experimental relation  $a \sim \omega^{-1}$ . Figure 6b shows that the piston has an acceptable response at 1Hz; at 2Hz the motion is still in phase with the laser signal, although the value of the amplitude is prompt to higher perturbations (see the error bars in figure 6c). At 4Hz (data not shown) the droplet motion starts to decouple from the heat signal, and at 8Hz the motion of the droplet resembles that observed at low frequencies, i.e., the coupling with the excitation frequency is completely lost. We believe that the maximum working frequency could be increased if smaller designs are achieved.

## 4 Conclusions

We have characterized the expansion/contraction processes of an air cavity, enclosed in a capillary and heated with a photoresponsive material. Aiming at using this system for microfluidic applications, we further demonstrated its operation as a valve and as a reciprocal actuator. The piston is easy to fabricate and can be in fact assembled in series using wire coating methods and the development of surface instabilities. The latter is allowed to develop in order to form the microheater zones, i.e., the deposition of the photoresponsive material at equally spaced spots along the capillary. We therefore envisage this wire coating technique as a “production line at the microscale”. Furthermore, unlike soft lithography and micromanipulation techniques, wire coating methodologies can be implemented in a straightforward manner in any laboratory. Interestingly, we found that the response time of the device, i.e., the speed at which the piston expands upon applying heat, improves as the overall apparatus size decreases. We also found that the kinematics of the expanded/contracted air can be modeled by using the well-known Kelvin-Voight unit used in the theory of viscoelasticity. In this sense, we explained the motion of the piston as a spring connected in parallel to

a dashpot and where the elastic response is attributed to the constant pressure at which the piston works; the retardation or viscous response, on the other hand, is attributed to the thermal relaxation time of the system.

The piston is able to work in phase with the excitation signal at different frequencies, and we expect that frequencies beyond 1 Hz could be used if smaller piston sizes are constructed. Future work will be focused on attaching flexible polymeric cantilevers to the capillary using soft lithography in order to test the piston as a positive displacement pump.

## 5 Acknowledgments

The authors appreciate financial support from Conacyt-México under grant 154464. R. Vélez specially acknowledge the financial support of Cátedras Conacyt.

## References

- 1 D. Baigl, *Lab Chip*, 2012, **12**, 3637–3653.
- 2 Y.-F. Chen, L. Jiang, M. Mancuso, A. Jain, V. Oncescu and D. Erickson, *Nanoscale*, 2012, **4**, 4839–4857.
- 3 V. R. Horowitz, D. D. Awschalom and S. Pennathur, *Lab Chip*, 2008, **8**, 1856–1863.
- 4 D. McGloin, *Phil. Trans. R. Soc. A*, 2006, **364**, 3521–3537.
- 5 D. Laser and J. Santiago, *J. Micromech. Microeng.*, 2004, **14**, R35–R64.
- 6 J. min Li, C. Liu, Z. Xu, K. ping Zhang, X. Ke, C. yu Li and L. ding Wang, *Lab Chip*, 2011, **11**, 2785–2789.
- 7 N. S. Lynn and D. S. Dandy, *Lab Chip*, 2009, **9**, 3422–3429.
- 8 M. Zimmermann, H. Schmid, P. Hunziker and E. Delamarche, *Lab Chip*, 2007, **7**, 119–125.
- 9 K. Iwai, K. C. Shih, X. Lin, T. A. Brubaker, R. D. Sochol and L. Lin, *Lab Chip*, 2014, **14**, 3790–3799.
- 10 Y. Zheng, W. Dai and H. Wu, *Lab Chip*, 2009, **9**, 469–472.
- 11 M. J. Kim and K. S. Breuer, *Small*, 2008, **4**, 111–118.
- 12 R. Soong, G. Bachand, H. Neves, A. Olkhovets, H. Craighead and C. Montemagno, *Science*, 2000, **290**, 1555–1558.
- 13 A. Jonáš and P. Zemánek, *Electrophoresis*, 2008, **29**, 4813–4851.
- 14 F. V. de Pol, H. V. Lintel, M. Elwenspoek and J. Fluitman, *Sensor Actuator*, 1990, **A21-A23**, 198–202.
- 15 J. Tsai and L. Lin, *J. Microelectromech. Syst.*, 2002, **11**, 665–671.
- 16 M. A. Unger, H.-P. Chou, T. Thorsen, A. Scherer and S. R. Quake, *Science*, 2000, **288**, 113–116.
- 17 W. H. Grover, R. H. C. Ivester, E. C. Jensen and R. A. Mathies, *Lab Chip*, 2006, **6**, 623–631.
- 18 W. Gu, X. Zhu, N. Futai, B. S. Cho and S. Takayama, *PNAS*, 2004, **101**, 15861–15866.
- 19 A. Terray, J. Oakey and D. W. Marr, *Science*, 2002, **296**, 1841–1844.
- 20 T. Ikegami, R. Ozawa, M. Stocker, K. Monaco, J. T. Fourkas and S. Maruo, *J. Laser Micro/Nanoengineering*, 2013, **8**, 6–10.
- 21 D. Palima and J. Glückstad, *Laser Photonics Rev.*, 2012, **7**, 478–494.
- 22 S. Maruo and H. Inoue, *Appl. Phys. Lett.*, 2006, **89**, 144101–3.
- 23 J. Leach, H. Mushfique, R. di Leonardo, M. Padgett and J. Cooper, *Lab Chip*, 2006, **6**, 735–739.
- 24 K. Ladavac and D. G. Grier, *Opt. Express*, 2004, **12**, 1144–1149.
- 25 R. Day and H. Stone, *J. Fluid Mech.*, 2000, **416**, 197–216.
- 26 M. T. Matthews and Y. M. Stokes, *Int. J. Heat Fluid Fl.*, 2012, **33**, 22–34.
- 27 K. Hale, C. Clark, R. Duggan and B. Jones, *IEE Proceedings*, 1988, **135**, 348–352.
- 28 J. R. Vélez-Cordero, A. M. Velázquez-Benítez and J. Hernández-Cordero, *Langmuir*, 2014, **30**, 5326–5336.
- 29 A. M. V. Benítez, M. Reyes-Medrano, J. Vélez-Cordero and J. H. Cordero, *accepted for publication in J. Lightwave Technol.*, 2014, **00**, 0.
- 30 D. Quéré, *Annu. Rev. Fluid Mech.*, 1999, **31**, 347–384.
- 31 J. H. Dumbleton and J. J. Hermans, *Ind. Eng. Chem. Fundam.*, 1970, **9**, 466–469.
- 32 P. Drazin, *Introduction to Hydrodynamic Stability*, Cambridge University Press, United Kingdom, 2002.
- 33 Y. B. Band, O. Kafri and P. Salamon, *J. Appl. Phys.*, 1981, **52**, 3745–3749.
- 34 Y. B. Band, O. Kafri and P. Salamon, *J. Appl. Phys.*, 1982, **53**, 8–28.
- 35 F. Mainardi and G. Spada, *Eur. Phys. J. Special Topics*, 2011, **193**, 133–160.
- 36 J. Maxwell, *Philos. T. Roy. Soc.*, 1867, **157**, 49–88.